## Accepted Manuscript

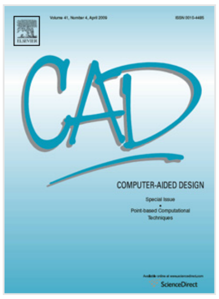

Efficient slicing procedure based on adaptive layer depth normal image

Long Zeng, Lip Man-Lip Lai, Di Qi, Yuen-Hoo Lai, Matthew Ming-Fai Yuen

PII: S0010-4485(11)00145-X
DOI: 10.1016/j.cad.2011.06.007
Reference: JCAD 1794

To appear in: *Computer-Aided Design*

Received date: 10 March 2011
Accepted date: 14 June 2011

- An efficient construction algorithm for RP layered model is proposed based on LDNI.
- Solid is converted into LDNI representation which is a layered and ordered point cloud.
- Boolean operation is performed on 1D segment in LDNI.
- Loops are constructed according to three simple rules.
- Mesh with 2 million triangles can be sliced in 2.5 seconds.

# Efficient Slicing Procedure based on Adaptive Layer Depth Normal Image

Long ZENG, Lip Man-Lip LAI, Di QI, Yuen-Hoo LAI, Matthew Ming-Fai YUEN
Department of Mechanical Engineering, Hong Kong University of Science and Technology, Hong Kong SAR, P.R. China

**Abstract**:
In layered modeling for rapid prototyping of products, compromising slicing accuracy and time is a critical issue. Based on adaptive Layer Depth Normal Image (LDNI), this paper proposes an efficient algorithm to achieve this compromise for complex Constructive Solid Geometry (CSG) models. First, each primitive at the tree leaf is converted adaptively into a LDNI solid whose Boolean operation can be performed efficiently. Then, a layered model is constructed directly from the Booleaned LDNI solid since it is actually a set of layered and ordered point cloud. In addition to speed, efficient use of memory is also taken into account in design of the adaptive LDNI algorithm. The capability and efficiency of this slicing algorithm are demonstrated by examples.

**Keywords**: rapid prototypes, layer manufacturing, layer depth normal image, constructive solid geometry.

## 1. Introduction

Rapid prototyping (RP) is an important technology in support of product development. In a RP process, a solid model is created and sliced into layers and output to a RP machine via a STL model. As a STL model is a piecewise approximation of a solid model, there exists a trade-off problem: accuracy and efficiency. Accuracy issue arises in RP when a solid model surface is tessellated. This can be controlled by the chordal error [1] which is the maximum shape difference between the tessellated model and the original model. The efficiency is mainly the time cost of slicing algorithm in preparing the data for layer-by-layer deposition. As slicing algorithms for STL model are based on triangle-plane intersection algorithms, the accuracy and efficiency trade-off is apparent when the tessellated elements increase. Such trade-offs can be highlighted in complex tessellated CSG models such as the ring model shown in Fig. 1a. The model is tessellated with a chordal error of 2$\mu$m, the total number of triangles is 1102632. In conventional RP procedure, a mesh-based Boolean operation need to be performed first (Fig. 1b) before it is sliced into a layered model (Fig. 1c). However, the mesh Boolean process is usually time-consuming, and the resulted Boolean model could be ill-constructed with defects, such as gaps, degenerated facets, etc.

LDNI [2] generates a layered point cloud model. It is an extension of LDI (Layered Depth Image) by assigning a unit normal vector to each of the sampled intersection points. LDI shoots an array of rays against the solid model and registers the multiple intersection points for each ray [3]. It can equally apply to a mesh model or a surface model efficiently with acceleration of standard graphic cards using standard OpenGL functions [4].

In this paper, an efficient adaptive LDNI slicing algorithm is proposed to achieve a compromising solution for the aforementioned trade-off problem. Firstly, adaptive Boolean operation is applied to the 1D segments of the adaptive LDNI sampled solids. Secondly, layered loop construction is applied to the Booleaned LDNI solid consisting of layered ordered point cloud.

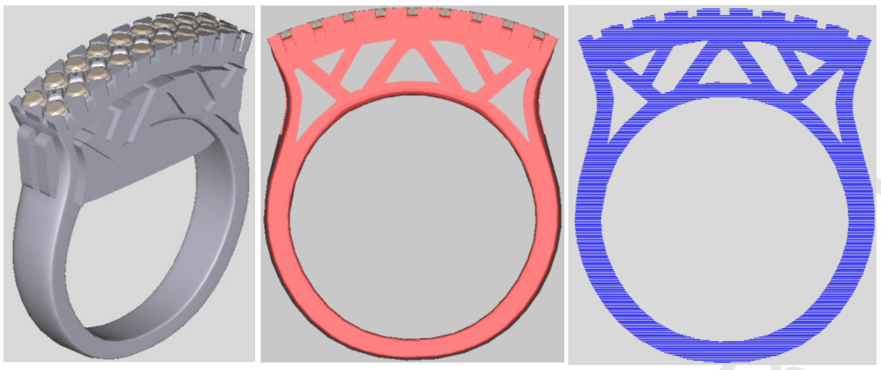

Fig. 1. Normal slicing procedure for a CSG ring model: (a) original model before Boolean; (b) Booleaned model; (c) sliced model

Section 2 of the paper reviews the related work on the slicing technique. An overview of the adaptive LDNI slicing algorithm is presented in section 3. The two major components of the adaptive LDNI slicing algorithm, adaptive LDNI Boolean and layered-loop construction, are detailed in section 4 and section 5 respectively. Efficiency of the algorithm is discussed in section 6 with support of examples. Finally, section 7 gives a summary and future work.

## 2. Related work

Rapid prototyping is an efficient technology to convert a digital model to a physical model using the layered deposition technique [5]. The slicing procedure is an integral step of the RP process, consisting of model creation, slicing, path generation, layer-by-layer deposition, and post processing [6]. STL model is the most commonly form of RP input. In preparing a layered model, the accuracy and efficiency are always the major concern. The solutions addressing this concern can be generally classified into four categories.

The first category is adaptive slicing, which enhances the slicing efficiency by reducing the number of layers. The adaptive slicing algorithm generates a variable slicing thickness given the local surface geometry or a given smoothness requirement. Dolenc and Makela [7] proposed the cusp height, which is a widely accepted concept, to describe the maximum deviation in RP manufacture. Within the user given maximum allowable cusp height, the thickness of current layer is predicted by point normal around the boundary of the last horizontal plane. Sabourin et al. [8] adopted the cusp height as a criteria and computed each slab thickness by recursive subdivision until the layers thickness under a given tolerance. This was further extended by Yan et al. [9], who obtained a higher efficiency using a non-uniform cusp height as a criteria. Mani et al. [10] proposed a region-based adaptive slicing, where the given model surface is classified into critical surfaces which are adaptively sliced, and non-critical surfaces, such as part interior, which are sliced using the maximum allowable layer thickness. Although adaptive slicing can alleviate the staircase quality problem and improve the slicing efficiency, the approximation error still exists during the tessellation step. Thus, adaptive slicing techniques are always used in combination with direct slicing techniques (see the hybrid category for more details).

The second category is direct slicing, which generates contours directly from the original input model without any model representation conversion. It avoids the approximation error that happens in the tessellation step. For NURBS models, Rajagopalan et al. [11] proposed a direct slicing method using the complete geometric representation. For freeform surfaces, Chakraborty et al. [12] output a layered file directly based on a surface-plane intersection algorithm. For point cloud models, Liu et al. [13] proposed an error-based segmentation method for direct RP. The point cloud data is first subdivided into regions and feature points are identified in each region. These feature points are used to construct an intermediate point-based curve model, where the RP layer contours are directly extracted. This method is further improved by Kumbhar [14] and applied to reverse engineering. The point cloud considered by Liu et al. and Kumbhar is unordered. However, in practice, points in some model representations are ordered and layered, such as the point cloud from medical scanning (see section 4.1). Whatever the input, be it a STL model; a surface model or a CSG model, it can be efficiently converted into a LDNI model with controllable conversion error using built-in graphic card acceleration.

The third category is extra-interpolation slicing, which usually fits the layered polygon contour with a biarc curve or a NURBS curve to improve the contour precision [15]. To reduce errors between the fitting curve and the sectional curve sliced from the original CAD model, Zhao et al.[16, 17] proposed a two-step method. The first step is to compute an interpolation curve to approximate the original curve in its normal section using the position of the two vertices and their tangent vectors. Then, points of the slice contour are obtained by calculating the intersection points between the interpolation curve and the slice plane.

The last category is the hybrid slicing algorithms, which are combinations of the above three slicing techniques. Since direct slicing technique can avoid the major approximation error occurring in the tessellation process and the adaptive slicing technique can improve the slicing efficiency, they are usually combined. Wu et al. [18] proposed an adaptive slicing algorithm for point cloud data. It projects all points between two consecutive horizontal planes into a mid-plane. These projected plane-points are then fitted by a polygon curve and the shape error is expressed as the distances between the points and the polygon curve. If the computed shape error is less than a user-defined threshold, then the current layer thickness is increased until this shape error is very close to the threshold value. However, the shape error definition is not invariant under point density. Yang et al. [19] and Qiu et al. [20] proposed an adaptive slicing algorithm based on curvature information of a MLS (Moving Least Square) surface. For NURBS surface, Ma et al. [21] also combined an adaptive scheme according to surface curvature information.

The proposed adaptive LNDI algorithm has the ability to directly slice CSG solids robustly and efficiently. Similar work was done by Sashidhar et al. [22], which constructs a layered model directly by computing planar analytic intersection curves while hierarchically traversing the CSG tree. Their method is limited to several regular CSG primitives since it is time-consuming to compute an analytic intersection between a free form model and a plane. Yan and Gu [23] proposed a more efficient method based on a ray tracing technique, where the intersection between a ray and a primitive were computed efficiently. This idea was further extended by W. K. Chiu, et al. [24] and W. M. Zhu et al. [25], where each primitive is represented in a ray representation, *dexel*. Thus, the Boolean operation for *dexel* model is also simplified from 3D to 1D segments Boolean operation. The proposed adaptive LDNI algorithm has the advantage over these algorithms in that each CSG primitive is represented as an adaptive LDNI, which have sample point normal information to enhance the algorithm's robustness. An additional advantage is the proposed algorithm is memory efficient as adaptive LDNI only stores each primitive's sample points in its own range.

In the proposed adaptive LDNI slicing algorithm, the input model is assumed to be a homogeneous object while discussion of slicing technique for heterogeneous objects can be found in [26]. The slicing direction in the proposed prototype system can be set manually to axis-aligned direction or automatically after Byun et al. [27].

## 3. Overview

For resolving the above compromising issue, a new slicing procedure based on adaptive LDNI is proposed. The algorithm requires a preset slicing direction and consists of two steps which are illustrated with a simple CSG tree model shown in Fig. 2:

- Adaptive LDNI Boolean
  Each component in the CSG model (Fig. 2a) is converted into a LDNI solid, adaptively (Fig. 2b) assisted by graphic card acceleration. The depth and normal information of each intersection point between the LDNI ray and the primitive are read directly from the pixel's depth and color buffer respectively. Thus each component can be tessellated with small approximation error and minimum loss of efficiency as no triangle-triangle intersection computation is necessary. Instead, the traditional 3D mesh Boolean operation is converted into 1D segments Boolean operation. It is more robust since the normal information in LDNI solid can help the point membership classification process (Fig. 2c).
- Layered loop construction
  Since the input point cloud from the first stage is a layered, ordered, and classified point cloud (IN: red point; OUT: green point, shown in Fig. 2c), each layer-loop can be easily obtained by connecting the points with the assistance of the 1D neighborhood information (Fig. 2d). The 1D neighborhood information is derived from the universal continuous principle (introduced in section 5).

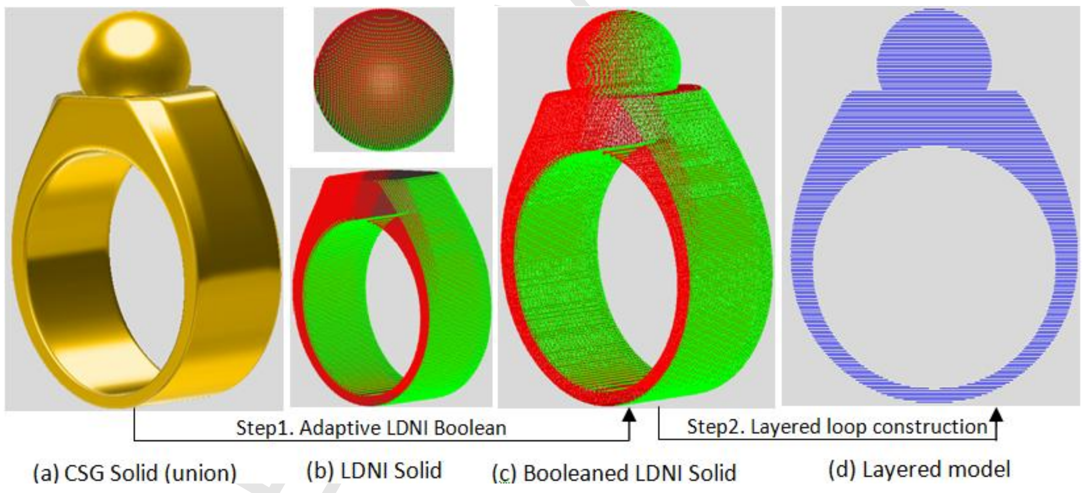

Fig. 2. Overview of the efficient slicing procedure based on adaptive LDNI

Compared with the previous mesh based slicing procedure under the same accuracy, the efficiency of the proposed slicing algorithm is manifested by its lower storage and much less time to generate a layered model (in .SLC file format) for fabrication, even for a complex CSG product.

## 4. Adaptive LDNI Boolean

Suppose the input model is a faceted surface model whose tessellation is controlled by chordal error λ (shown in Fig. 3a), defined as the Hausdorff distance between the tessellated model and the original model. The facet number will increase dramatically when λ decreases. For a sphere with radius 1mm shown in Fig. 3b to Fig. 3c, the mesh facet number increased from 1572 faces to 20052 faces while λ is changed from 0.01mm to 0.001mm. Thus, an efficient LDNI Boolean operation with slicing procedure is introduced, which is dependent on the ray resolution but almost independent of the facet number.

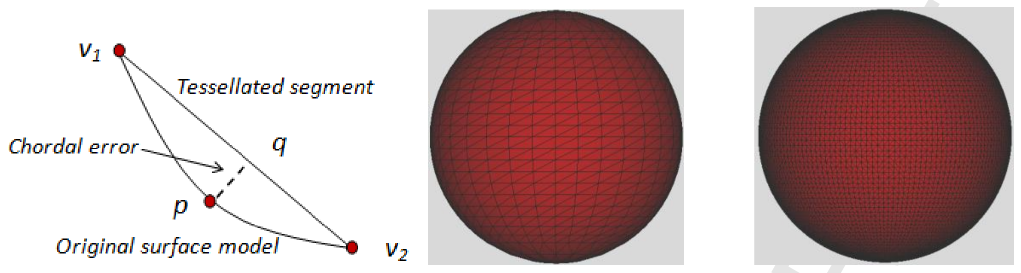

(a) Chordal error λ (b) λ=0.01mm, 1572 faces (c) λ=0.001mm, 20052 faces

Fig. 3. Chordal error based tessellation for a sphere with a radius of 1mm

## 4.1. Adaptive LDNI solid

LDNI solid is a layered point cloud model constructed efficiently with the help of a graphic card's rendering pipeline. First, it renders the input model under a special rendering configuration. Then it is sampled with a certain resolution, denoted as LDNI resolution. In practice, LDNI resolution is represented by two variables: layer thickness, $D_{layer}$, and ray width, $D_{ray}$. As shown in Fig. 4a, if the left-bottom point of the sphere's Enlarged Bounding Box (EBB) is (0, 0) and right-top point is (*Width*, *Height*), then the view-port is a screen rectangle which contains an array of *Total_rays* rays in the horizontal direction and *Total_layers* layers in the vertical direction. The *Total_rays* and *Total_layers* are computed by

, (1)

Where *Width* and *Height* are the width and height of the EBB. In the following example, the rendering environment configuration is specified by LDNI resolution, *Width*, and *Height*.

The unsorted depth and normal value is read from the depth buffers and color buffers. A detailed view of the *i*th layer in Fig. 4b shows that the depth value and the normal vectors (blue arrow at point A and B) are retrieved. The coordinates (x, y, z) of a sample point A on the *j*th ray in the *i*th layer can be computed as:

$$x = j\,/Total\_rays * Width \text{ of EBB} \quad (2)$$

$$y = depth\ value\ of\ A * Depth \text{ of EBB} \quad (3)$$

$$z = i\,/Total\_layers * Height \text{ of EBB} \quad (4)$$

Where *Depth* is the depth of the EBB.

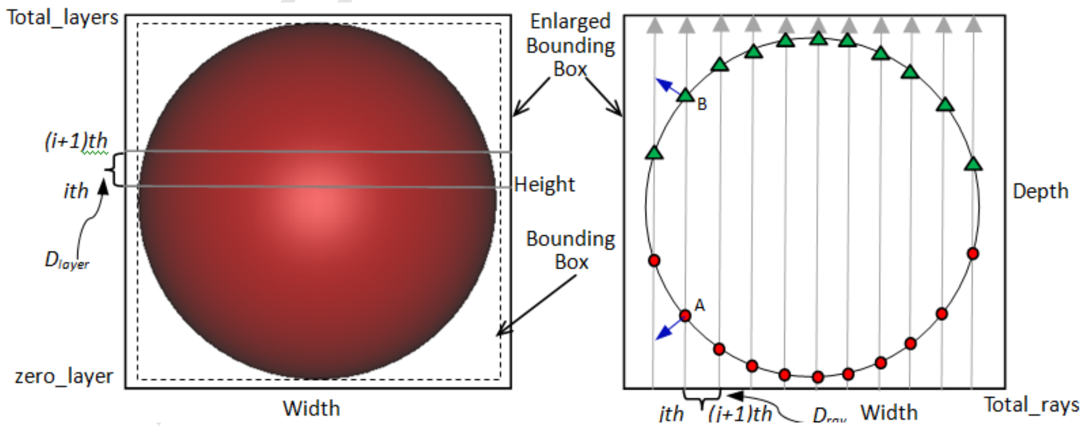

(a) (b)

Fig. 4. Adaptive LDNI solid generation. (a) Rendering environment setup, ray direction is perpendicular with the paper; (b) detailed view of the *i*th layer (IN: circular point; OUT: triangular point).

In this paper, there are several major modifications compared to the previous LDNI techniques [2, 3, 28] since it is applied to slicing procedure.

Firstly, a single LDNI is adopted instead of the original three LDNIs (x-LDNI, y-LDNI, and z-LDNI) for speed efficiency. This is because a much higher resolution is used (800*800 in most cases) in the slicing procedure. Though some small features (gap or thin-shell) will be lost, this is acceptable in RP since such a small feature cannot be processed in RP.

Secondly, the original LDNI is modified into a memory efficient technique, denoted as adaptive LDNI. In a CSG model with multiple components, the **Normal LDNI** adopts the Global EBB (GEBB), as shown in Fig. 5, which contains all the components instead of the LBB (Local Bounding Box). And the ray correspondence is automatically created. However, the amount of memory space required by each LDNI solid becomes a problem when the component number increases. For example, for a sphere in 800*800 LDNI resolution (this resolution is normal in our projects), the data from depth buffer (4 bytes) and color buffer (3 bytes) need to be stored in a LDNI solid. The storage needed is about 4.5MB (Megabytes). If the CSG model is composed of 400 components and each component needs two depth buffers (at least), 3600MB will be required to store the LDNI solids. This is a considerable burden for desktop computers (this component scale is not unusual in items such as jewelry design). Therefore, the **Adaptive LDNI** is proposed to store only the necessary information for each component. Taking the CSG model shown in Fig. 5 for example, it contains components A, B, and C. For each component, when it is converted into a LDNI solid, only the data whose corresponding pixel contained in its LBB is stored. Thus, our scheme is to create a map between the GEBB and LBBs. This can be easily achieved by recording a pair of index (*rayStartIndex, layerStartIndex*) for each LBB. Such as for C component,

*rayStartIndex*—the ray index in GEBB of the ray which first intersect with C.

*layerStartIndex*—the layer index in GEBB of the layer which first intersect with C.

Then, the corresponding global position of the *i*th local ray in C can be computed by (*rayStartIndex* +*i*) th ray.

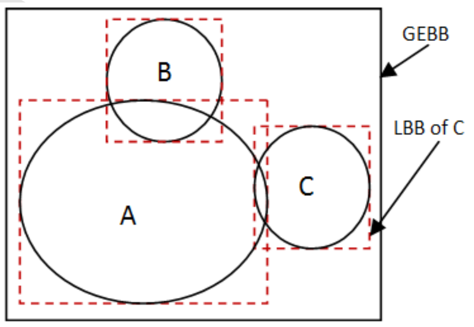

Fig. 5. Adaptive LDNI converts an object in its LEBB instead of the GEBB.

Thirdly, intersection points are classified into IN/OUT with the help of normal information from LDNI (this is similar to the method used in *dexel* model [24, 25]). As shown in Fig. 4b, the blue arrows are the unit normal vectors of the sample points, and the gray arrow is the ray direction. If the dot product between a sample point's normal vector and the ray direction vector is less than zero, then this sample point is colored as IN (circular red color, such as sample point A); otherwise, it is classified as OUT (triangular green color, such as sample point B). These classified points are useful in the loop construction step.

## 4.2. LDNI Boolean

The LDNI Boolean is performed layer-by-layer and ray-by-ray. The 1D ray Boolean operation is computed by hierarchically traversing the CSG binary tree. The ray intersection mainly consists of three steps (shown in Fig. 6): firstly, classify the end points of intervals $r_A(i, j)$ with respect to the intervals $r_B(i, j)$ as outside/inside; intervals $r_A(i, j)$ means the intervals on the *i*th ray of the *j*th layer of primitive A. Secondly, do the same classification for the end points of $r_B(i, j)$ with respect to the intervals $r_A(i, j)$. Finally, construct the resultant intervals according to the following rules:

- If $r_A(i, j)$ *union* $r_B(i, j)$, *keep the outside end points of both* $r_A$ *and* $r_B$.
- If $r_A(i, j)$ *intersect* $r_B(i, j)$, *keep the inside end points of both* $r_A$ *and* $r_B$.
- If $r_A(i, j)$ *subtract* $r_B(i, j)$, *keep the outside end points of* $r_A$ *and inside end points of* $r_B$.
- If $r_B(i, j)$ *subtract* $r_A(i, j)$, *keep the outside end points of* $r_B$ *and inside end points of* $r_A$.

The outside/inside classification is only conducted on the *Depth* coordinate since the rays with the same global index have the same width and height coordinates. Thus, is considered inside the interval when and ; is outside the interval when and , where =10e-4 is chosen in our implementation. The special cases happen when or . However, this can be handled easily using the neighborhood information [29] with the help of normal information of each sample point. An illustration of the LDNI Boolean operation is given in Fig. 6.

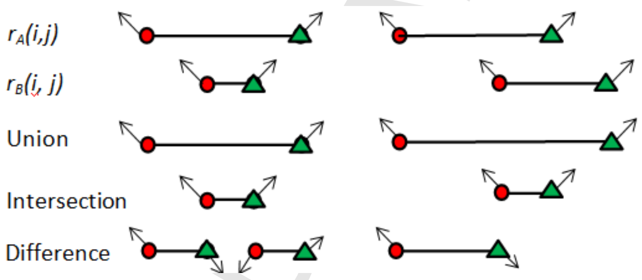

Fig. 6. Ray Boolean operation (IN: circular point; OUT: triangular point)

Fig. 7 is a simple example demonstrating the application of the adaptive LDNI solid and LDNI Boolean operation introduced in this section. Since the LDNI solid is constructed by putting a single camera at the scene (left to right in this example), some of the points in the perpendicular direction at the base of the Athena model (Fig. 7a) are lost (Fig. 7b and Fig. 7c). However, this can be handled successfully in the post loop construction process.

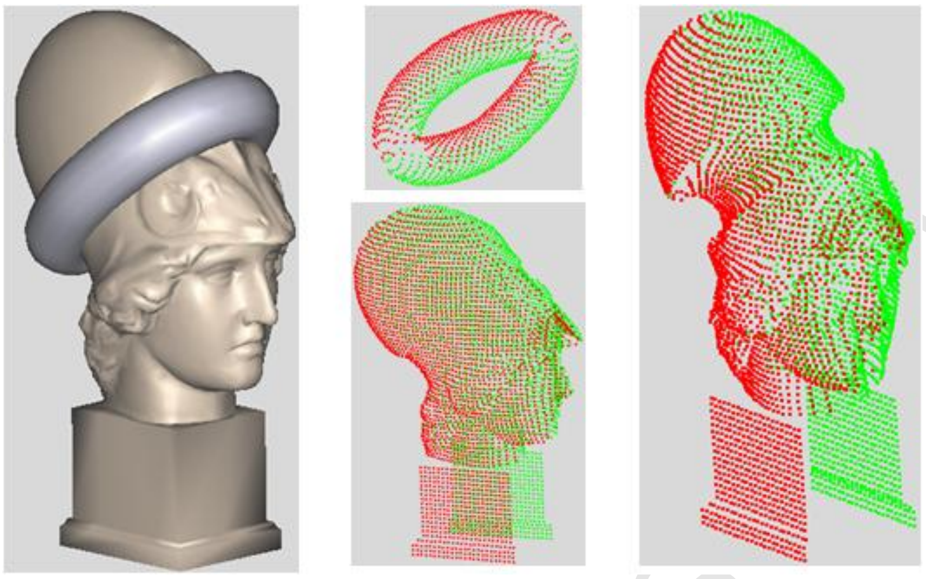
(a) Athena subtract torus (b) LDNI solids (c) LDNI Boolean result

Fig. 7. LDNI Boolean results of Athena subtracting a torus

## 5. Loop construction

The main purpose of loop construction is to find the correct connectivity for each sample point.

### 5.1. Rules for loop construction

Several simple rules are proposed to lay down the mathematical foundation for loop construction.

***Definition 1*** **Continuous 1D-neighborhood**: On a line (Fig. 8a), the continuous 1D -neighborhood for a reference point is an open interval, which is the intersection between the line and an open disk centered with the given point and radius .

According to the continuity definition in calculus, the point number in its -neighborhood is infinite and if the reference point is tagged, there exists a small positive value , and all the points in the -neighborhood must have the same point type with the reference point.

If this definition is extended to a 1D discrete set, we get

***Definition 2*** **Discrete 1D-neighborhood**: In a discrete set on a line (Fig. 8b), the discrete 1D -neighborhood for a reference point is a finite point set, where is the sample resolution with .

Here, is to guarantee that a point's -neighborhood is not an empty set. For the case of a partial neighborhood, either the left- or right-neighborhood may be empty. In such case, the reference point is called the turning point, such as the points on the first or last ray. This case will be handled differently in the loop construction process. Thus, similar properties for the reference point can be derived from definition 2:

- If a reference point is an internal point, there exists one left and one right nearest point having the same point type as the reference point.
- If a reference point is a turning point, there exists one left or one right nearest point having the same point type as the reference point.

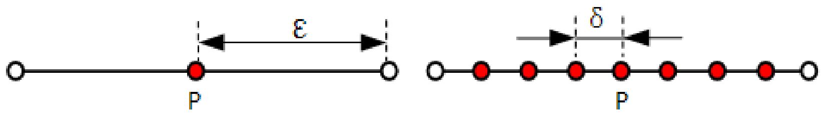

Fig. 8. 1D-neighborhood for (a) continuous and (b) discrete cases

Now, three simple rules for loop construction are introduced.

***Rule 1*** **Manifold principle**: the input model is a valid manifold mesh model.

Manifold mesh model means each ray must intersect the model even times (even number of times) and each point must have two connections to its left and right point. A valid manifold mesh model further restricts the input model to have no small features whose dimensions are less than the sample resolution . Otherwise, these small features will be ignored in the resulting RP model. The resolution is chosen to be better than the accuracy of most major RP machines. Additionally, this rule also implies the given model has a consistent orientation. It is important since the normal is used for the point type classification and to improve the algorithm robustness.

***Rule 2*** **1D-neighborhood principle**: In a valid manifold model, a point on an internal ray may find its two connections at the two nearest neighborhood points on adjacent rays with the same point type (IN or OUT) under the prerequisite that there are no other points between them.

A simple illustration of this principle is shown in Fig. 9. $P_1P_2$ is a valid connection. However, $P_1P_3$ is not since $P_4$ is located between $P_1$ and $P_3$. In a LDNI solid, the principle can be derived from definition 2 and rule 1.

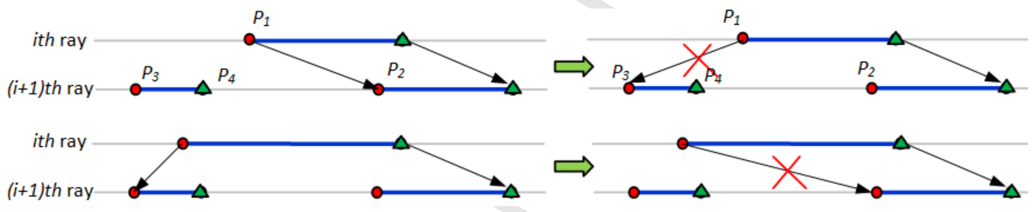

(a) Correct connection (b) Incorrect connection

Fig. 9. Find point connectivity using the 1D-neighborhood principle

In order to find the two connections of a turning point, we have,

***Rule 3*** **Half 1D-neighborhood principle**: for a turning-point, one connection can be found on its left or right next ray according to *rule 2*. The other connection can be found on the nearest point on the same ray.

As shown in Fig. 10a, one of the connections of the turning-point $P_1$ is found, point $P_3$, on the next ray according to *rule 2*, and the other, point $P_2$, is found on the same ray according to *rule 3*.

## 5.2. Loop construction

Before constructing the loops in each layer, the connections of each point are found. Since the input is a manifold model (rule 1), each point should only have two pointers: pre and post. If a CSG model has multiple loops in a single layer, it may be difficult to detect the turning-points. A better way is first finding the pre and post pointers for each point according to rule 2. Then, the connectivity of each point is checked. If its connections are less than two, we apply rule 3. After these two steps, each point (shown in Fig. 10a) can find valid points as its pre and post connections. If there are still points whose connections are less than two, they will be considered as invalid points and ignored (this may happen if the model has some defects).

After the connections of each point are found, loops are constructed by tracing the point's connectivity information, as shown in Algorithm 1.1. The neighboring point in a loop is connected with a polyline, as shown in Fig. 10b.

```
Algorithm 1.1 Layer-loop-construction
While (there is still an unused point)
    Create a new loop, $L_{new}$.
    Start point, $P_s$, is selected as an arbitrary point, and flagged as used.
    Do
        The next point $P_n$ = $P_s$->post.
        If $P_n$ is not NULL and unused
            Add to the new loop $L_{new}$ and flag as used.
    While ($P_n$ not equal $P_s$)
```

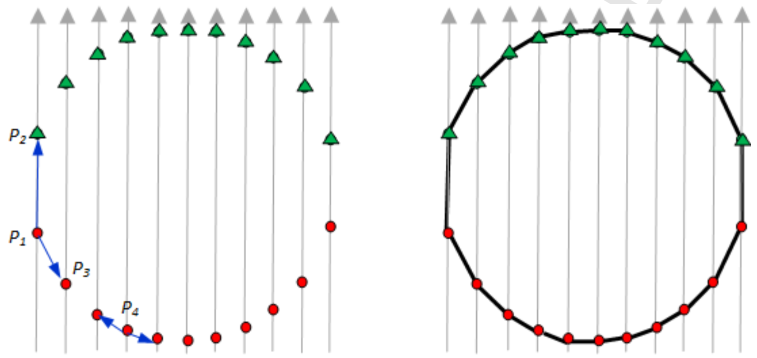

(a) Find connections according to rule 2 and rule 3 (b) Connected loop

Fig. 10. Loop construction for one layer of the sphere in Fig. 4

## 6. Experimental results and discussions

This slicing algorithm has been tested in the commercial software JewelCADPro [30]. Several tests are used to demonstrate the main features of this algorithm (Note that all the tests mentioned in this paper are run on a Window XP system PC with Intel® Core™ i5 CPU750@2.67GHz, 2.86GHz, and 3GB RAM).

$T_C$ is the time used to convert all primitives to adaptive LDNI solids according to the method described in section 4.

$T_L$ is the time used to construct the layered loops using the method described in section 5.

$T_T$ is the total time cost, equal to $T_C$ plus $T_L$.

The slicing direction can be selected from one of the standard axes for models in JewelCADPro.

This section starts with some examples to show the main features of our algorithm. Then it is applied to two complex CSG models to demonstrate the algorithm's capability and efficiency. We also compare the speed of our algorithm with that of InfinySlice [31] and Rhinoceros [32]. The *Width*, *Height*, and LDNI resolution for each example model are given. The unit for each model's dimension is in millimeters (mm). For RP process, it is useful that the layer number can be computed indirectly from the parameters given. In the efficiency comparison of the algorithms, the layer number for the output layer model is adjusted to be equal.

### 6.1. Examples

The first feature is that the algorithm's speed efficiency is almost independent of the mesh density which relates to the chord error. This is tested and verified by the ring model shown in Fig. 11. The LDNI resolution is fixed to 0.0762mm*0.0762mm and the mesh density is varied (Fig.

11b). The algorithm time cost is listed in Table 1. From the table, the conversion time $T_C$ increases marginally since the LDNI solid conversion process needs to access all the face information on the original mesh model. However, the time cost on loop construction $T_L$ is almost constant since it only depends on the node number of the LDNI solid, which is only controlled by sample resolution. Therefore, the original surface model can be tessellated finely to decrease the approximation error while having little reduction in slicing efficiency. This model is also used to compare the algorithm efficiency against Rhinoceros, and InfinySlice.

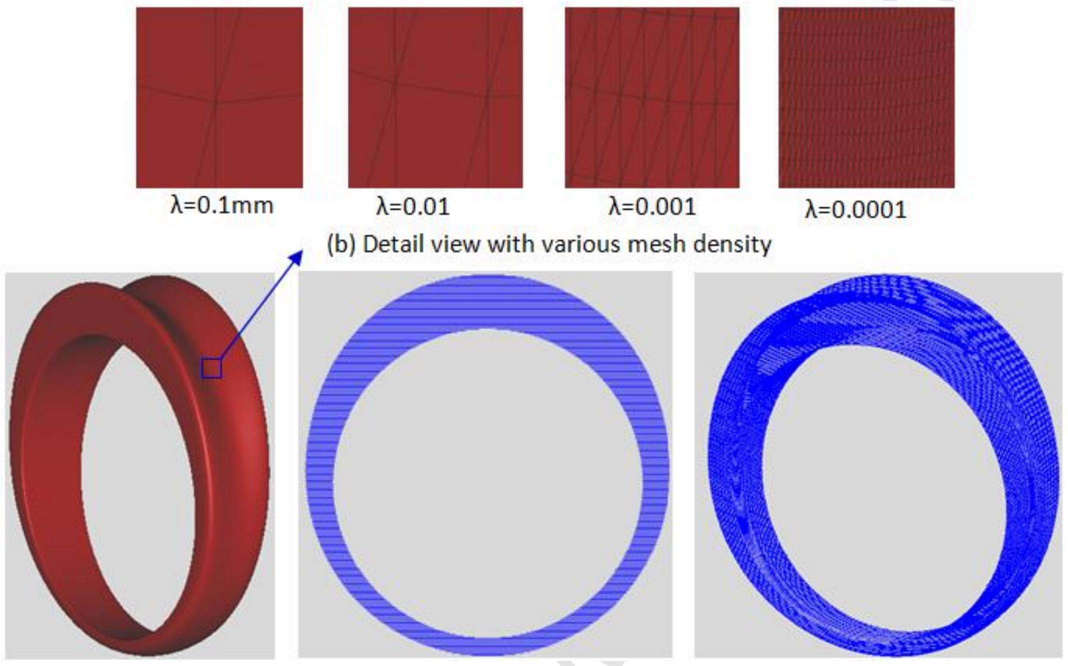

(a) Original model (c) Sliced model-front view (d) Sliced model-3D view

Fig. 11. A ring model is used to test the effects of chordal error (λ) on the algorithm speed (LDNI resolution: 0.0762mm*0.0762mm; Width is 19.96mm, Height is 21.0mm)

Table 1 Statistical data of Fig. 11 to show the effects of mesh density (LDNI resolution: 0.0762*0.0762)

| λ (mm) | Triangle # | Our algorithm | | | InfinySlice | Rhinoceros |
|---|---|---|---|---|---|---|
| | | $T_C$ (s) | $T_L$ (s) | $T_T$ (s) | $T_T$ (s) | $T_T$ (s) |
| 0.1 | 1,530 | 0.109 | 0.188 | 0.297 | 1 | < 1 |
| 0.01 | 17,308 | 0.156 | 0.172 | 0.328 | 2 | 2 |
| 0.001 | 113,692 | 0.266 | 0.187 | 0.453 | 5 | 13 |
| 0.0001 | 1,401,978 | 2.313 | 0.187 | 2.500 | 13 | 106 |

The second feature is that the LDNI resolution is a key factor affecting the slicing algorithm efficiency. This is tested by the horse model shown in Fig. 12. From the statistics given in Table 2, we know that the layer construction time $T_L$ is almost proportional to the LDNI resolution. When the LDNI resolution becomes nine times finer, from 0.0381*0.0381 to 0.0127*0.0127, the layer construction time increases about nine times, from 485ms to 3984ms. This is because the layer construction algorithm introduced in section 5 has linear complexity with respect to the intersection point number which is determined by LDNI resolution. The LDNI conversion time $T_C$ also increases since the conversion process not only depends on model's mesh complexity, but also on the LDNI resolution since an LDNI solid mainly stores the depth and normal information which is proportional to the LDNI resolution. In the following example models are tessellated by chordal error λ=0.001.

The third feature is the algorithm can be applied to a complex CSG model and its primitives. As shown in Fig. 13, the proposed slicing algorithm is directly applied to the complex CSG model (Fig. 13a). Since it has 55 primitives, the total number of mesh triangle is 1.2 million if each primitive is tessellated with a chordal error λ=0.0001. This will take several hours for the mesh-based Boolean operation. However, the proposed slicing algorithm can output a RP model (.SLC file) in about 11 seconds. In the implementation, there are two methods to create a CSG Boolean tree. One is to select the entity pair, and then assign a Boolean operator to them but without carrying out the actual Boolean operation. The other is to perform actual Boolean operation using a very coarse mesh and record the Boolean operation order in a CSG Boolean tree. Another CSG example is shown in Fig. 16.

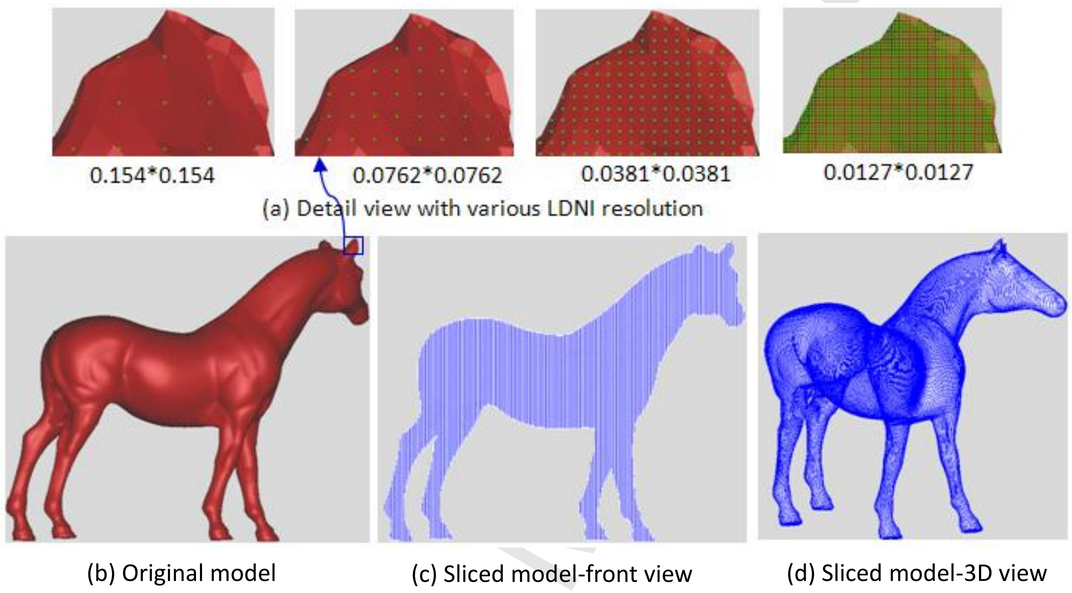

Fig. 12. A horse model is used to test the effects of LDNI resolution on the algorithm speed (LDNI resolution: 0.0762*0.0762; *Width* is 19.25mm, *Height* is 16.04mm)

Table 2. Statistical data of Fig. 12 to show the effects of LDNI resolution on the algorithm speed

| LDNI resolution (mm) | $T_C$ (ms) | $T_L$ (ms) | $T_T$ (ms) |
|---|---|---|---|
| 0.1524*0.1524 | 359 | 63 | 422 |
| 0.0762*0.0762 | 406 | 140 | 546 |
| 0.0381*0.0381 | 562 | 485 | 1047 |
| 0.0127*0.0127 | 2328 | 3984 | 6312 |

The fourth feature is that the algorithm is memory efficient. Compared with the Normal LDNI, the adaptive LDNI is much more memory efficient since only the necessary information is stored in each LDNI solid. This is a more obvious problem when it is applied to complex CSG models with many small primitives/components, such as Fig. 13 and Fig. 16. Their memory usage is given in Table 3. In addition, the algorithm speed also has minor improvements since the 1D segment Boolean only performed in the local EBB area.

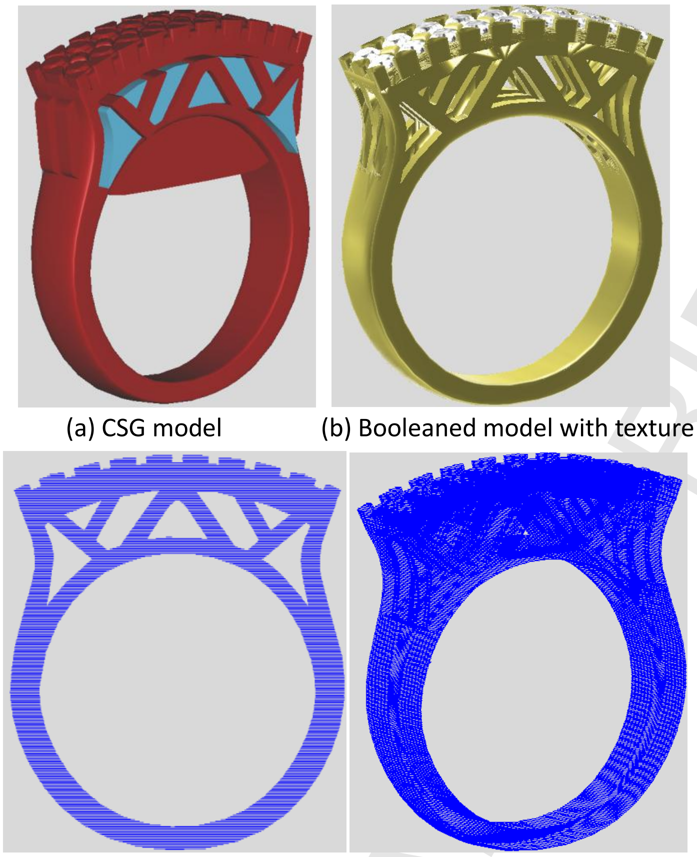

(a) CSG model (b) Booleaned model with texture

(c) Sliced model-front view (d) Sliced model-3D view

Fig. 13. A ring model composed of 55 components (LDNI resolution: 0.0762*0.0762; *Width* is 20.61mm, *Height* is 24.40mm)

Table 3 Storage and speed comparison between Normal LDNI and Adaptive LDNI

| Model | LDNI resolution (mm) | Normal LDNI | | Adaptive LDNI | |
|---|---|---|---|---|---|
| | | $T_T$ (s) | RAM(MB) | $T_T$ (s) | RAM(MB) |
| Fig. 13 | 0.1524*0.1524 | 5.4 | 6.45 | 4.8 | 0.39 |
| | 0.0762*0.0762 | 10.5 | 27.26 | 10.1 | 1.89 |
| | 0.0381*0.0381 | 32.3 | 130.47 | 28.0 | 8.95 |
| | 0.0127*0.0127 | 232.3 | 1289.03 | 215.7 | 86.50 |
| Fig. 16 | 0.1524*0.1524 | 4.3 | 1.38 | 4.0 | 0.05 |
| | 0.0762*0.0762 | 5.1 | 5.6 | 4.9 | 0.25 |
| | 0.0381*0.0381 | 7.3 | 22.12 | 6.5 | 1.11 |
| | 0.0127*0.0127 | 26.6 | 216.11 | 19.4 | 10.38 |

To illustrate the application of the adaptive LDNI slicing algorithm, the sliced model of two commonly used benchmark models “Angel” and “Happy Buddha” are shown in Fig. 14 and Fig. 15.

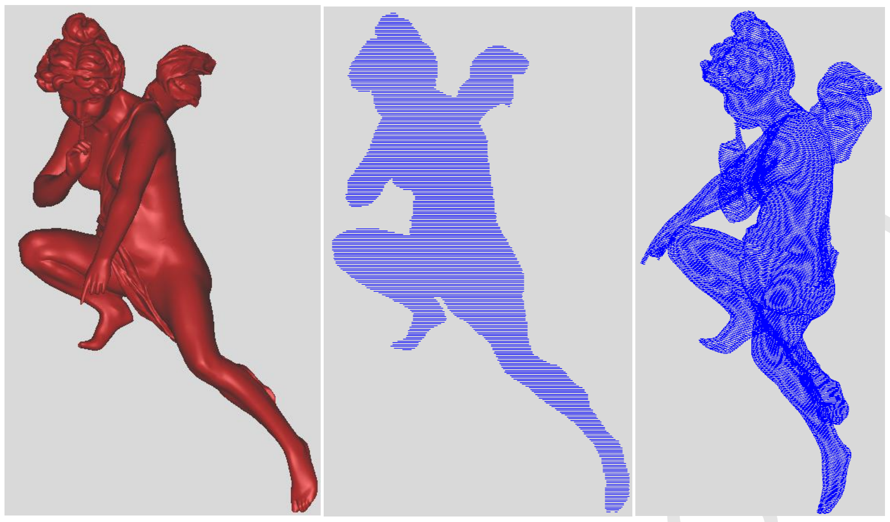

Fig. 14 Sliced Angel model (LDNI resolution: 0.0762*0.0762; *Width* is 14.88mm, *Height* is 22.09mm)

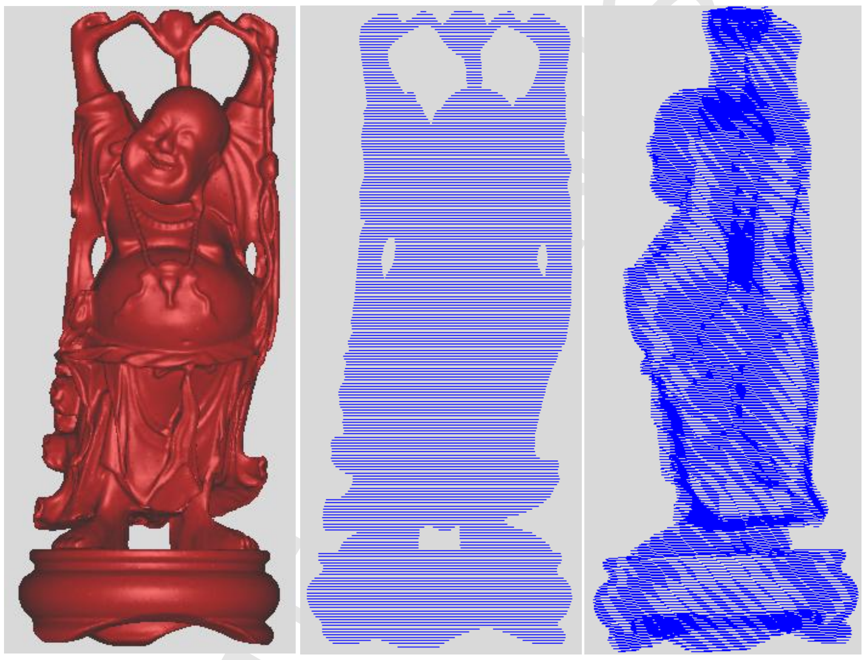

Fig. 15 Sliced Happy Buddha model (LDNI resolution: 0.0762*0.0762; *Width* is 7.68mm, *Height* is 11.64mm)

## 6.2. Comparison

The speed of our slicing algorithm is compared with the slicing algorithm of InfinySlice and Rhinoceros 4.0. InfinySlice is a popular and efficient slicer. Rhinoceros is selected since it has the same NURBS library openNURBS [33] with our test prototype JewelCADPro, which may minimize the data access difference. Both software packages have the same layered model output format (.SLC file).

The simple ring model shown in Fig. 11 is selected as the test model since the slicing algorithm in InfinySlice and Rhinoceros are not designed for CSG solid. The ring model is tessellated under different chordal errors and exported as STL files from JewelCADPro. They are imported to InfinySlice and Rhinoceros 4.0 evaluation version. All exported .SLC files have the same layers and the same file size. The output .SLC file size in JewelCADPro can be adjusted by an extra smooth parameter. Thus, we can make the exported .SLC files have the same size under the same layer thickness. The time cost in InfinySlice is read directly from its statistical data and the time cost in Rhinoceros 4.0 is estimated from the clock since there is no way to read it directly.

Based on above configuration, the time cost is listed in Table 1. The slicing algorithm in InfinySlice is hardware optimized (parallel computation using multi-core technique) and it is much faster than Rhinoceros. But it is about 10 times slower than the proposed algorithm. The slicing algorithm in Rhinoceros is mesh based, i.e. intersection points are computed by intersecting the mesh model with a set of horizontal planes. The time cost of the slicing algorithm depends on the mesh complexity. This is also verified by the data in Table 1. However, the mesh complexity has much less effect on the proposed algorithm. From Table 1, it also can be found that the proposed algorithm is more efficient than that of InfinySlice and Rhinoceros. It is about 10~30 times faster than Rhinoceros for normal mesh complexity (10 thousand to 100 thousand triangles). If the mesh number increases, this difference will be even larger.

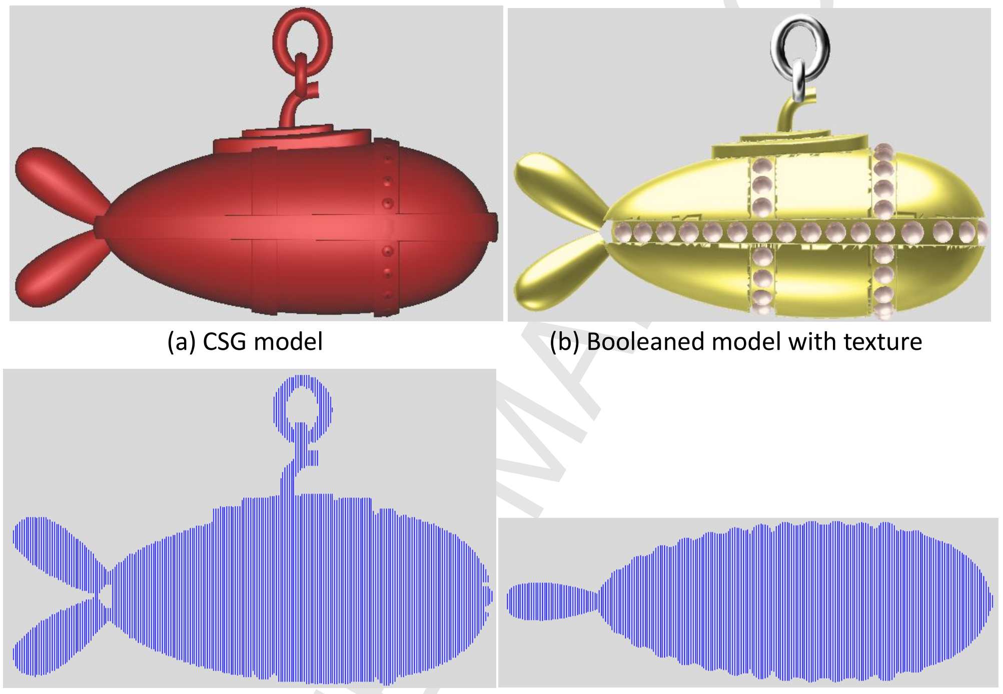
(a) CSG model (b) Booleaned model with texture

(c) Sliced model-front-view (d) Sliced model-bottom-view

Fig. 16. A submarine pendant made up of 74 components (LDNI resolution: 0.0762*0.0762; *Width* is 11.51mm, *Height* is 7.36mm)

## 6.3. Discussions

In a CSG model with *m* primitives, the memory complexity for Normal LDNI is , where is the maximal depth buffer number, and are the maximum layer and ray number computed from the global enlarged bounding box. Usually, parameter *m* and are much less than . and usually have the same magnitude. In the worst case, i.e. and , the memory cost for the slicing procedure is bi-quadratic. Adaptive LDNI has a similar complexity in the worst situation. However, its total memory cost is equal to , where are all local values of the *i*th primitive. In most cases, are much less than , thus, the memory usage of adaptive LDNI is much more efficient than normal LDNI.

The approximation error during the tessellation process is a major error source for the previous mesh-plane intersection based slicing algorithms. The proposed algorithm can successfully alleviate this issue efficiently despite introducing a new LDNI resolution error which is controllable. These points are sampled at a certain resolution (sample error). The proposed algorithm can strike a compromise and obtain a high speed in very fine LDNI resolution. The examples in the paper have clearly demonstrated this.

## 7. Summary and future work

This paper focuses on alleviating the classic trade-off problem between approximation error and algorithm efficiency in rapid prototyping. Our method is based on the LDNI solid representation. The LDNI solid representation is actually a layered and order point cloud model, which has two major advantages in slicing procedure: first, the Boolean operation can be reduced to 1D segment Boolean operation which can be performed efficiently and robustly; second, it simplifies the layered model construction in the slicing procedure.

In the proposed adaptive LDNI algorithm, first convert each primitive into an LDNI solid adaptively which is accelerated by the graphic card. Then, the 1D Boolean operation on the LDNI solid is performed efficiently. Finally, the two connections of each point are obtained according to the three prescribed rules and loops are generated efficiently based on each intersection point's connectivity. The normal information in LDNI solid is useful in two aspects: support intersection classification and resolving special cases in Boolean operation. In addition, the algorithm is also memory efficient since only the necessary data for each primitive/component is stored. The efficiency of this algorithm has been demonstrated by applying not only to a single object, but also to a complex CSG object.

One future improving direction is the topology-preserving slicing procedure with the help of normal information in LDNI solid representation. In the current algorithm, if an object has a thin gap less than the LDNI resolution and this gap is parallel to the current ray direction, it will be ignored. This will lead to a wrong topology in the output layered model.

**Acknowledgement**

The jewelry models of Fig.1, Fig.2, Fig.11, Fig.13, and Fig.14 are exported from the database of JewelCADPro software. The work in this paper is partially supported by Jewellery CAD/CAM Ltd. [30]. The first author is also grateful to Dr. S. L. Siu and Edmond Li of Jewellery CAD/CAM Ltd. for the stimulating discussions leading to this research, particularly Dr. S. L. Siu's original contribution to rule 2 for the loop construction.

## References

[1] R. Jamieson and H. Hacker, "Direct slicing of CAD models for rapid prototyping," *Rapid Prototyping Journal,* vol. 3, pp. 12-19, 1995.

[2] C. C. L. Wang and Y. Chen, "Layered depth-normal images: a sparse implicit representation of solid models," *Computing Research Repository,* 2007.

[3] J. Shade*, et al.*, "Layered Depth Images," presented at the Computer graphics and interactive techniques, 1998.

[4] *OpenGL*. Available: http://www.opengl.org/

[5] A. Pang*, et al.*, "A CAD/CAM system for process planning and optimization in LOM (Laminated Object Manufacturing)," *IIE Transactions (Institute of Industrial Engineers),* vol. 33, pp. 345-355, 2001.

[6] P. M. Pandey*, et al.*, "Slicing procedures in layered manufacturing: a review," *Rapid Prototyping Journal,* vol. 9, pp. 274-288, 2003.

[7] A. Dolenc and I. Mäkelä, "Slicing procedures for layered manufacturing techniques," *Computer-Aided Design,* vol. 26, pp. 119-126, 1994.

[8] E. Sabourin*, et al.*, "Adaptive slicing using stepwise uniform refinement," *Rapid Prototyping Journal,* vol. 2, pp. 20-26, 1996.

[9] J. Q. Yan*, et al.*, "Adaptive direct slicing with non-uniform cusp heights for rapid prototyping," *The International Journal of Advanced Manufacturing Technology,* vol. 23, pp. 20-27, 2004.

[10] K. Mani*, et al.*, "Region-based adaptive slicing," *CAD Computer Aided Design,* vol. 31, pp. 317-333, 1999.

[11] B. Susila*, et al.*, "Interfacing geometric model data with rapid prototyping systems," *Journal of Intelligent Manufacturing,* vol. 10, pp. 323-329, 1999.

[12] D. Chakraborty and A. R. Choudhury, "A semi-analytic approach for direct slicing of free form surfaces for layered manufacturing," *Rapid Prototyping Journal,* vol. 13, pp. 256-264, 2007.

[13] G. H. Liu*, et al.*, "Error-based segmentation of cloud data for direct rapid prototyping," *Computer-Aided Design,* vol. 35, pp. 633-645, 2002.

[14] V. K. Kumbhar*, et al.*, "Improved intermediate point curve model for integrating reverse engineering and rapid prototyping," *International Journal of Advanced Manufacturing Technology,* vol. 37, pp. 553-562, 2008.

[15] B. Koc*, et al.*, "Smoothing STL files by Max-Fit biarc curves for rapid prototyping," *Rapid Prototyping Journal,* vol. 6, pp. 186-203, 2000.

[16] J. Zhao*, et al.*, "A computing method for accurate slice contours based on an STL model," *Virtual and Physical Prototyping,* vol. 4, pp. 29-37, 2009.

[17] Z. Zhao and L. Laperrière, "Adaptive direct slicing of the solid model for rapid prototyping," *International Journal of Production Research,* vol. 38, pp. 69-83, 2000.

[18] Y. Wu, "Modelling cloud data using an adaptive slicing approach," *Computer-Aided Design,* vol. 36, pp. 231-240, 2004.

[19] P. Yang and X. Oian, "Adaptive slicing of moving least squares surfaces: Toward direct manufacturing of point set surfaces," *Journal of Computing and Information Science in Engineering,* vol. 8, pp. 0310031-03100311, 2008.

[20] Y. Qiu*, et al.*, "Direct slicing of cloud data with guaranteed topology for rapid prototyping," *The International Journal of Advanced Manufacturing Technology,* 2010.

[21] W. Ma*, et al.*, "NURBS-based adaptive slicing for efficient rapid prototyping," *Computer-Aided Design,* vol. 36, pp. 1309-1325, 2004.

[22] G. Sashidhar, "a method to generate exact contour files for solid freeform fabrication," in *Solid Freeform Fabrication Symposium*, University of Texas at Austin, 1992, pp. 95-101.

[23] Y. Xue and G. P, "A review of rapid prototyping technologies and systems," *Computer-Aided Design,* vol. 28, pp. 307-318, 1996.

[24] W. K. Chiu and S. T. Tan, "Using dexels to make hollow models for rapid prototyping," *CAD Computer Aided Design,* vol. 30, pp. 539-547, 1998.

[25] W. M. Zhu and K. M. Yu, *Dexel-based direct slicing of multi-material assemblies* vol. 18. London, ROYAUME-UNI: Springer, 2001.

[26] X. Y. Kou and S. T. Tan, "Data structure and algorithms for virtual prototyping of heterogeneous objects," *Computer-Aided Design and Applications,* vol. 3, pp. 59-67, 2006.

[27] H. S. Byun and K. H. Lee, "Determination of optimal build direction in rapid prototyping with variable slicing," *International Journal of Advanced Manufacturing Technology,* vol. 28, pp. 307-313,

2006.

[28] H. Bruno*, et al.*, "Volumetric collision detection for deformable objects," ed, 2003.

[29] A. A. G. Requicha and H. B. Voelcker, "Boolean operations in solid modeling: Boundary evaluation and merging algorithms," *Proceedings of the IEEE,* vol. 73, pp. 30-44, 1985.

[30] *Jewellery CAD/CAM Ltd*. Available: http://www.jewelcadpro.com

[31] *InfinySlice*. Available: http://www.marcam.de/cms/index.126.en.html

[32] *Rhinoceros*. Available: http://www.rhino3d.com/

[33] *openNURBS*. Available: http://www.opennurbs.org